ϕ-meson production in proton-proton collisions

M. Büscher, M. Hartmann, Y. Maeda, R. Koch, H. Ohm, H. Ströher
Institut für Kernphysik, Forschungszentrum Jülich, D-52425 Jülich, Germany

J. Haidenbauer, A. Sibirtsev
Institut für Kernphysik ITP, Forschungszentrum Jülich, D-52425 Jülich, Germany

K. Nakayama
Department of Physics and Astronomy, University of Georgia Athens, Georgia 30602, USA

H. Müller
Institut für Kern- und Hadronenphysik, Forschungszentrum Rossendorf, D-01314 Rossendorf, Germany

V. Koptev, S. Mikirtychiants, M. Nekipelov
High Energy Physics Dept., Petersburg Nuclear Physics Institute, 188350 Gatchina, Russia

S. Dymov, V Komarov, V. Kurbatov
Joint Institute for Nuclear Research 141980, Dubna, Russia

A. Kacharava, M. Nioradze
High Energy Physics Institute, Tbilisi State University 380086 Tbilisi, Georgia

K. Pysz
The Henryk Niewodniczanski Institute of Nuclear Physics, PL-31342 Cracow, Poland

and the ANKE collaboration

Spokesperson: M. Hartmann (M.Hartmann@fz-juelich.de)

October 2001

Abstract

We request in total four weeks of beam time to measure ϕ-meson production in pp collisions at beam energies 2.65 and 2.70 GeV by detecting its decay into K^+K^- mesons. Our result combined with available SPES-III results on ω-meson production will provide information about OZI-rule violation at energies close to the ϕ-production threshold. The first two weeks are requested for spring 2002 at $T_p = 2.70$ GeV.

1 Motivation

Assuming ideal SU(3) octet-singlet mixing Okubo, Zweig and Iizuka proposed that the production of ϕ-mesons from initial non-strange states is substantially suppressed in comparison to ω production [1, 2, 3]. Due to SU(3) breaking octet and singlet states are mixed and the deviation from the ideal ϕ–ω mixing is $\alpha_V \simeq 3.7^\circ$ [4]. This leads to cross-section ratios for ϕ- and ω-meson production under similar kinematical conditions of [5, 6]:

$$R = \frac{\pi N \to \phi N}{\pi N \to \omega N} = \frac{NN \to NN\phi}{NN \to NN\omega} \simeq \tan^2 \alpha_V = 4.2 \times 10^{-3}. \qquad (1)$$

However, it may be possible a certain amount of hidden strangeness in the nucleon would manifest itself in a cross section significantly exceeding the limits given by the OZI rule.

ϕ and ω production in *pp* collisions has been investigated theoretically in many studies [7, 8, 9] by evaluating the diagrams depicted in Fig.1 within different approaches.

Considering the diagram of Fig.1a [7] under equivalent kinematical conditions for ϕ and ω production, the ratio R is given by the ratio of the $\pi N \to \phi N$ to $\pi N \to \omega N$ amplitudes squared ($|M_V|^2$) and can be evaluated from available data for the reaction cross section through

$$\frac{d\sigma}{d\Omega} = \frac{1}{64\pi^2 s} \frac{q_V}{q_\pi} |M_V|^2, \qquad (2)$$

where s is squared invariant πN collision energy and q_π, q_V are the pion and vector meson momenta in the cm system, respectively. The ratio $|M_\phi|^2/|M_\omega|^2$ is shown by Fig.1e) as a function of excess energy $\epsilon = \sqrt{s} - m_N - m_V$, where m_N and m_V are the nucleon and ϕ or ω masses, respectively. To calculate the ratio at the same excess energy, the data on $\pi N \to \omega N$ invariant amplitude was fitted by the function

$$|M| = 3.6 + 54.6 \exp(-1.21\epsilon), \qquad (3)$$

with ϵ taken in GeV. At excess energies $\epsilon < 300$ MeV the ratio of the $\pi N \to \phi N$ to $\pi N \to \omega N$ amplitudes squared can be well fitted by almost constant value of

$$R = (13.3 \pm 1.6) \times 10^{-3}. \qquad (4)$$

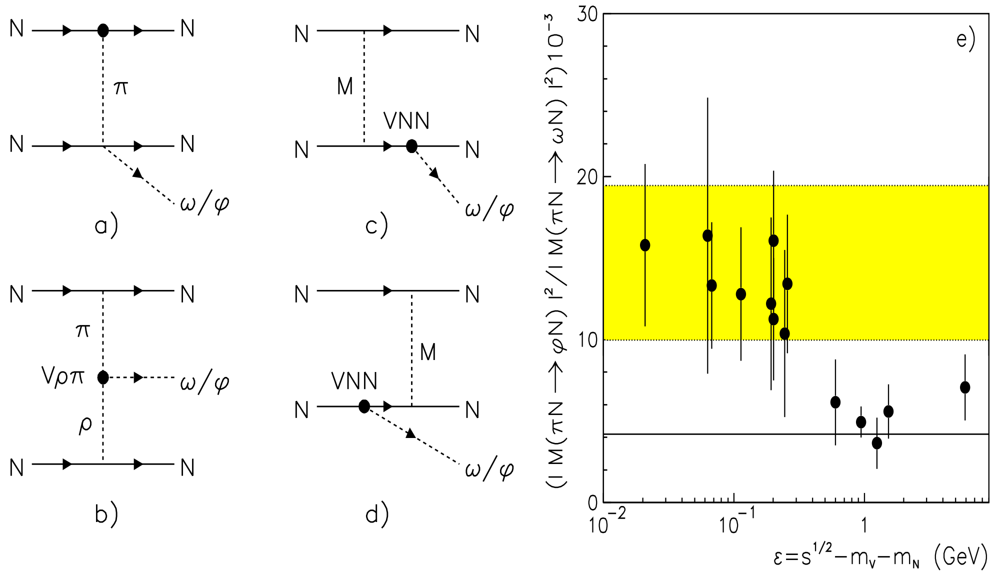

Figure 1: a-d) The diagrams for $NN\to NNV$ reactions with $V{=}\phi,\omega$ and M denoting NN interaction in the initial and final states. e) The ratio of the $\pi N\to\phi N$ to $\pi N\to\omega N$ amplitudes squared as a function of excess energies. Experimental data were taken from [10], the shaded area shows the uncertainty in the ratio of the $\phi\rho\pi$ to $\omega\rho\pi$ coupling constants, while the solid line indicates the ratio given by the SU(3) $\phi{-}\omega$ mixing angle.

Considering the mesonic currents given by the diagram of Fig.1b) [8, 9] the ratio R is given by the ratio of the $\phi\rho\pi$ to $\omega\rho\pi$ coupling constants squared. The $\phi\rho\pi$ coupling can be determined directly from the $\phi\to\rho\pi$ decay width giving $g_{\phi\rho\pi}{=}1.23{\pm}0.05$. The $\omega\rho\pi$ coupling can be evaluated [11] from the $\omega\to 3\pi$, $\omega\to\pi^o\gamma$ and $\rho\to\pi^o\gamma$ decay width and varies between $g_{\omega\rho\pi}=8.82{\pm}0.5$ and $12.32{\pm}3.12$. Consequently, the mesonic current diagram of Fig.1b) results in the ratio of ϕ to ω production cross section in pp collisions under similar kinematical conditions as

$$R{=}(9.97{\div}19.45)\times 10^{-3}, \tag{5}$$

which is indicated by the shaded area in the Fig.1e).

Considering the nucleonic currents shown by the diagrams of Fig.1c-d) the ratio R is given by the ratio of the ϕNN to ωNN coupling constants squared. The ωNN coupling is well fixed by the analysis [12, 13] of NN scattering

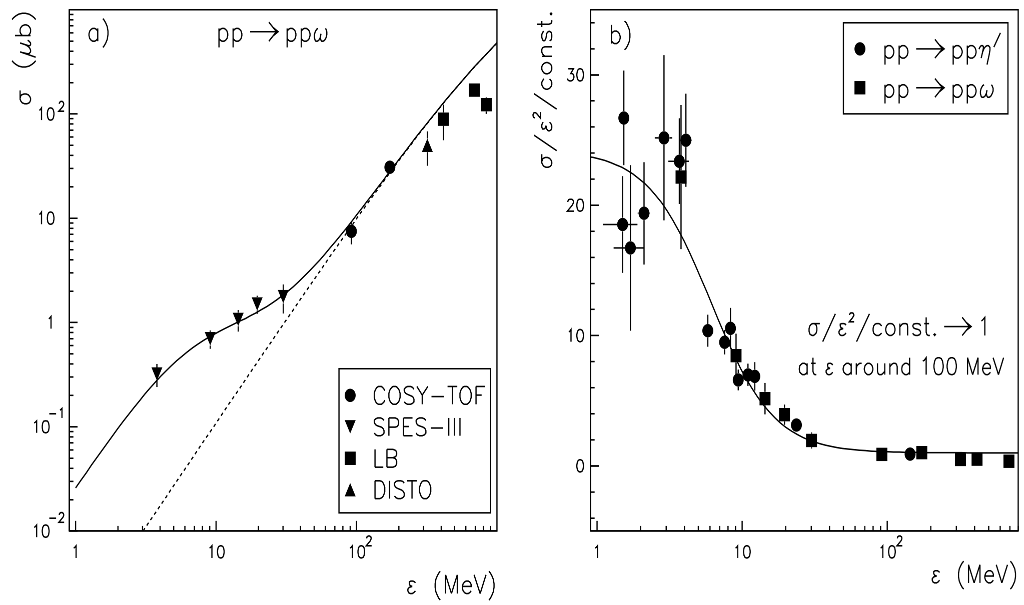

Figure 2: a) Total $pp \rightarrow pp\omega$ cross section as a function of excess energy [10, 14, 15, 16, 17]. The dashed line shows the phase space dependence of Eq.6, while the solid line includes the correction of Eq.7 due to pp FSI. b) The reduced $pp \rightarrow pp\omega$ and $pp \rightarrow pp\eta'$ cross section normalized to 1 at $\epsilon \simeq 100$ MeV. η' data are taken from [19, 20, 21, 22, 23]. The solid line shows the fit by Eq.7.

data resulting in $g_{\omega NN}$=11÷16. The ϕNN coupling is not well known and has been only estimated by SU(3) symmetry through Eq.1. Based on such an estimate for $g_{\phi NN}$, the ratio R of $\phi-$ to $\omega-$ meson production in pp collisions due to the diagrams of Fig.1c-d) alone will lead to R=4.2$\times 10^{-3}$.

However, as was found in Ref. [9], the interference between the mesonic and nucleonic currents, i.e. between the amplitudes given by diagrams of Fig.1b) and that of Fig.1c-d), might substantially influence the ratio of ϕ to ω production in pp collisions. The effect was found to be strong at energies close to the ϕ- and ω-production thresholds. Moreover, such an interference might lead to a strong energy dependence of the ratio R at $\epsilon \leq 100$ MeV, with $\epsilon = \sqrt{s} - 2m_N - m_V$, where $\sqrt{s}$ is invariant energy of the pp interaction.

Data [14, 15, 16, 17] on $pp \rightarrow pp\omega$ cross section are available over the wide range of excess energies ϵ and are collected in Fig.2a). At $\epsilon \geq 100$ MeV the data closely follow phase space behavior and the total reaction cross section

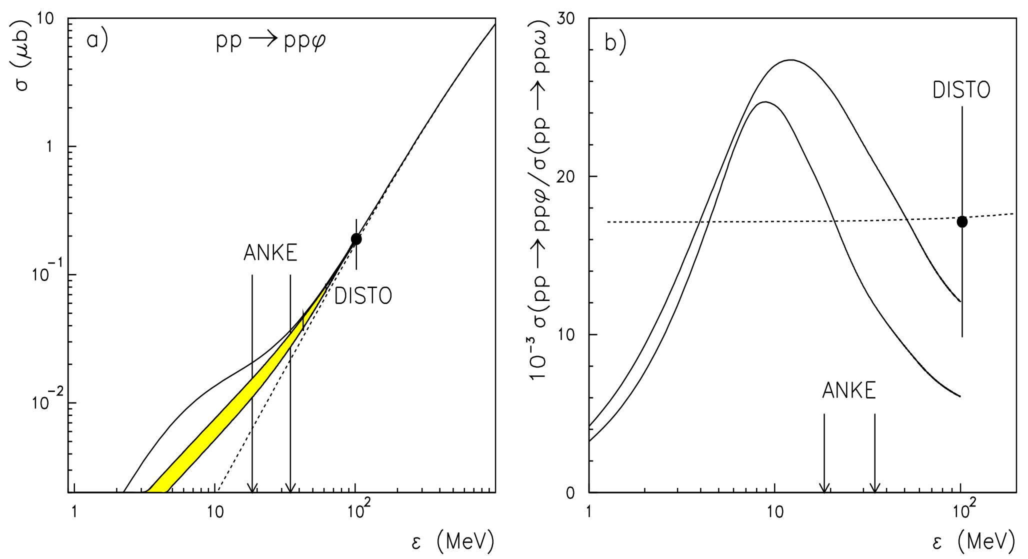

Figure 3: a) Total $pp{\rightarrow}pp\phi$ cross section as a function of excess energy. The DISTO result is taken from Ref.[16]. Dashed line shows the phase-space dependence of Eq.6, while the solid line includes the correction of Eq.7 due to pp FSI. Shaded area indicates uncertainties for the calculations of Ref.[9], which includes both mesonic and nucleonic currents. The arrows indicate the energies proposed for the ANKE measurements. b) The ratio of the $pp{\rightarrow}pp\phi$ to $pp{\rightarrow}pp\omega$ cross section as a function of excess energy ϵ. The solid line shows the prediction from Ref.[24] evaluated with different model parameters. The dashed line indicate the ratio given by Eqs.6,7. The ratio for the DISTO result was obtained by interpolating the data on $pp{\rightarrow}pp\omega$ cross section from Fig.2a) at the same ϵ.

can be well described as

$$\sigma = C_j \frac{(\sqrt{s} - 2m_N - m_V)^2}{s^2 - 4sm_N^2}, \tag{6}$$

with C_ω=5.5 mb·GeV^2. The parameterization of Eq.6 is shown in Fig.2a) by the dashed line. At ϵ<100 MeV the data substantially deviate from phase space due to strong pp final state interaction FSI.

It was proposed in Ref.[18] that energy dependence of the reaction cross section caused by the pp FSI is similar for the production of mesons with masses heavier the η-meson. This energy dependence can be directly evaluated from the available data on ω [14, 15, 16, 17] and η' [19, 20, 21, 22, 23] production. Fig.2b) shows the total $pp\to pp\omega$ and $pp\to pp\eta'$ cross section reduced by an energy dependence ϵ^2 due to the phase space and normalized to 1 around $\epsilon\simeq$100 MeV. The data indicate a similar energy dependence below $\epsilon\simeq$100 MeV and can be well described by

$$h(\epsilon) = 1 + \frac{23.2}{1+0.027\epsilon^2}, \tag{7}$$

where ϵ is given in MeV as is shown in the in Fig.2b) by the solid line. The solid line in the Fig.2a) indicates that the $pp\to pp\omega$ cross section can be well described by Eq.6 corrected by pp FSI of Eq.7.

Following these considerations one might expect a similar near-threshold energy dependence for the $pp\to pp\phi$ cross section. At low energy the $pp\to pp\phi$ reaction has only been measured at DISTO [16] and the resulting cross section is shown by the Fig.3a). The dashed line in the Fig.3a) shows the phase-space dependence of Eq.6 with C_ϕ=0.12 mb·GeV^2, while the solid line indicate the estimated $pp\to pp\phi$ cross section including the FSI correction of Eq.7.

Finally, following the estimation discussed above, the ratio R of the $pp\to pp\phi$ to $pp\to pp\omega$ cross sections should not depend on excess energy below $\epsilon\simeq$100 MeV and is given by $R\simeq$17 as shown by the dashed line in the Fig.3b). This ratio exceeds the SU(3) limit given by the $\phi-\omega$ mixing angle, but agrees with the data on $\pi N\to\phi N$ and $\pi N\to\omega N$ reactions as well as with the ratio of the $\phi\rho\pi$ to $\omega\rho\pi$ coupling constants, as is illustrated by the Fig.1e).

Fig.3b) also shows the ratio of the $pp\to pp\phi$ to $pp\to pp\omega$ cross section – both measured by DISTO – interpolated to the same excess energy by the data collected in the Fig.2a).

The microscopic calculations of Ref.[9] consider the contribution from the mesonic and nucleonic currents to ϕ and ω production in pp collisions and predict the $pp\to pp\phi$ cross section shown by the shaded area in Fig.2a). The size of the hatched area indicates the uncertainties due to model parameters. The model of Ref. [9] predicts the energy dependence of the $pp\to pp\phi$ cross section that is significantly different from the consideration of Eq.7. The solid lines in Fig.3b) show the predicted ratio of the $pp\to pp\phi$ to $pp\to pp\omega$ cross sections given in the Ref.[24] for different model parameters.

Summarizing, the ANKE measurements will clarify the situation with the ratio of the $pp\to pp\phi$ to $pp\to pp\omega$ cross section near the reaction threshold. Furthermore, the measurements at excess energies ϵ=18.5 and 34.6 MeV should resolve the uncertainties on the energy behavior of the $pp\to pp\phi$ cross section.

2 ANKE spectrometer and a new detection system for negatively charged particles

A detailed description of ANKE – which was specially designed for K^+ detection in large background conditions [27] – is given in [28], including the forward and backward detection systems. The new detection system for negatively charged particles [29, 30] is shown in Fig.4 within the full ANKE detector setup. The construction of the components is finished and the detector elements are currently being built. Table 1 shows the envisaged time schedule for installation of the different components of the negative particle detector.

Detector part	*Installation at ANKE*	*completion of implementation*
Start scintillators	done	done
Wire chamber 1 and 2	done	done
Stop scintillators 2	done	done
Stop scintillators 1	Week 51/2001	January/2002
Cherenkovs	Week 11/2002	March/2002

Table 1: Time schedule for the installation of the $K^-(\pi^-)$ detector.

The negative-particle detection system will be placed inside the return yoke of the C-shaped dipole D2 (magnetic stray fields up to $\approx$ 200 mT) and partly outside the magnet (Fig.4). It consists of two multi-wire proportional chambers (MWPCs) for precise tracking and momentum determination (Δp/p $\approx$ 2-3%) and of "start"- and "stop"- scintillators for TOF and ΔE measurement used for particle identification. At the maximum field strength of D2 ($\approx$ 1.6 T) negatively charged ejectiles can be measured in the momentum range from $\approx$ 120 to $\approx$ 1000 MeV/c. The horizontal and vertical angular acceptances are roughly: $\alpha_{hor} = \pm 12°$; $\alpha_{ver} = \pm 8°$ at 200 MeV/c and $\alpha_{hor} = -2°$ to $12°$, $\alpha_{ver} = \pm 5°$ at 1000 MeV/c.

For K^--detection in the experiment the expected major background components are negative pions from the target and protons scattered from the magnet yoke, the vacuum chamber and the detectors. This background ex-

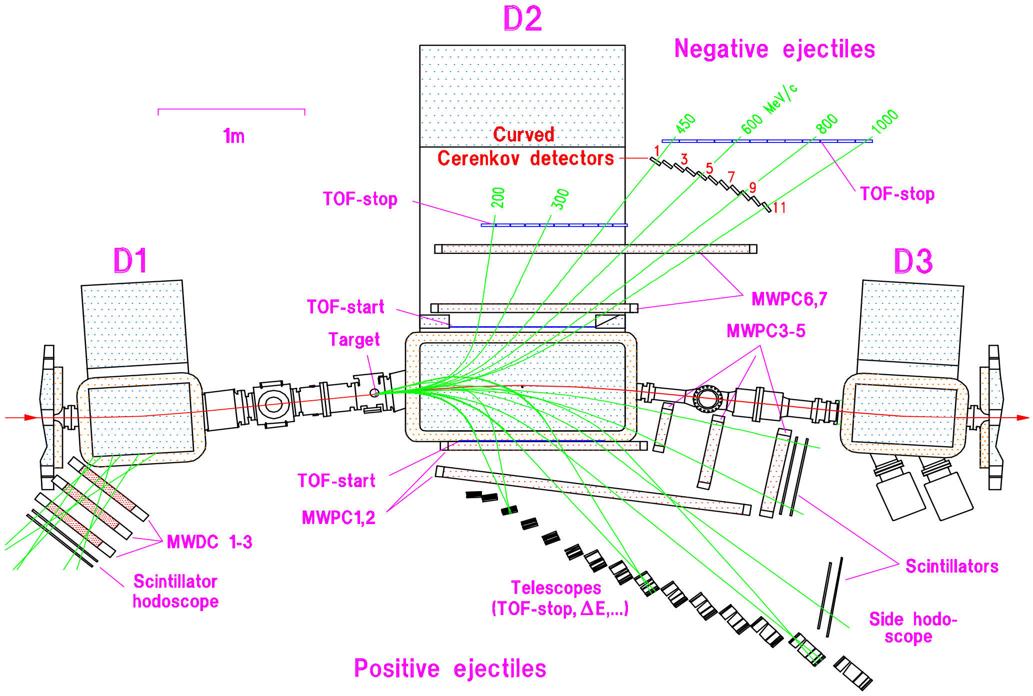

Figure 4: Schematic layout of the complete ANKE spectrometer. Left of the beam line (seen in beam direction) – partly inside the separation magnet D2 – the new detection system for the measurement of negatively charged ejectiles. Below the beam line the positive particle detection system with range telescopes optimized for K^+ detection. In forward direction – between D2 and D3 – a detector composed of 3 fast MWPCs and a scintillator wall is placed. An additional scintillator wall – the side hodoscope – is installed between the positive and forward system to cover the gap between these two groups.

ceeds the K^- intensity by some orders of magnitude. With a timing resolution of $\sigma \approx$240 ps (which has been archived for the positive particle side of ANKE), the measured time-of-flight allow reliable kaon-pion discrimination up to 500 MeV/c (ΔT$>$ 4σ). For higher momenta up to 1000 MeV/c the time-of-flight differences decrease to 2σ of the timing resolution (Table 2), in spite of the longer flight-paths to the "stop" scintillator group II.

Considering a pion background larger than 100:1, this difference is not sufficient for the separation. On the positive particle side, additional background reduction is achieved by the measurement of energy losses and ranges in the focal surface of the D2 magnet after degradation of the particle ener-

p $[MeV/c]$	d $[cm]$	$TOF\ \pi^-$ $[ns]$	$TOF\ K^-$ $[ns]$	ΔTOF $[ns]$
500	175	6.06	8.20	2.14
600	175	5.99	7.55	1.57
800	201	6.80	7.87	1.07
1000	215	7.24	7.99	0.76

Table 2: Time differences between kaons and pions for higher momenta.

gies. In the high momentum region of negative ejectiles the energies are too large and the focal surface is far off, making the use of degraders impossible. For detection of very weak K^+ intensities background suppression was most efficiently achieved through the detection of delayed muons from the decay of stopped K^+-mesons. This method cannot be applied for K^- identification. K^--mesons at rest are captured to form kaonic atoms, whose lifetime is too short to produce signals of measureable delay.

For these reasons more sophisticated Cherenkov detectors will be installed at the negative-particle side [31]. The aim is to use them as veto counters in which only pions will produce a detectable signal. The counters consist of bars made of lucite which are slightly bent. The advantage of such differential Cherenkov detectors is an optimal separation between K^- and π^-. Figure 5 demonstrates the principle of operation of the curved counters.

For an appropriate radius of curvature of ≈ 2.4 m the particle angle with the detector front surface varies only by less than $1°$ along the detector. For a straight detector element this variation would amount to $10°$, depending on the momentum region. Simulations were carried out in which realistic momentum and angular distributions of the particle trajectories were taken into account [31]. The production and propagation of Cherenkov light in the detector was calculated. The results show that due to the spread of the horizontal components of the angles of particle incidence, also K^- mesons may produce Cherenkov light which reaches the PMTs. However the intensity of the detected "Kaon light" amounts to less than 3% of the intensity of "pion light". These numbers do not change drastically when statistical fluctuations of the light production and propagation processes are taken into account. Both, calculations and test measurements have shown that even for detectors of a thickness of only 2 cm, pion-kaon separation for particles coming from the target can be achieved.

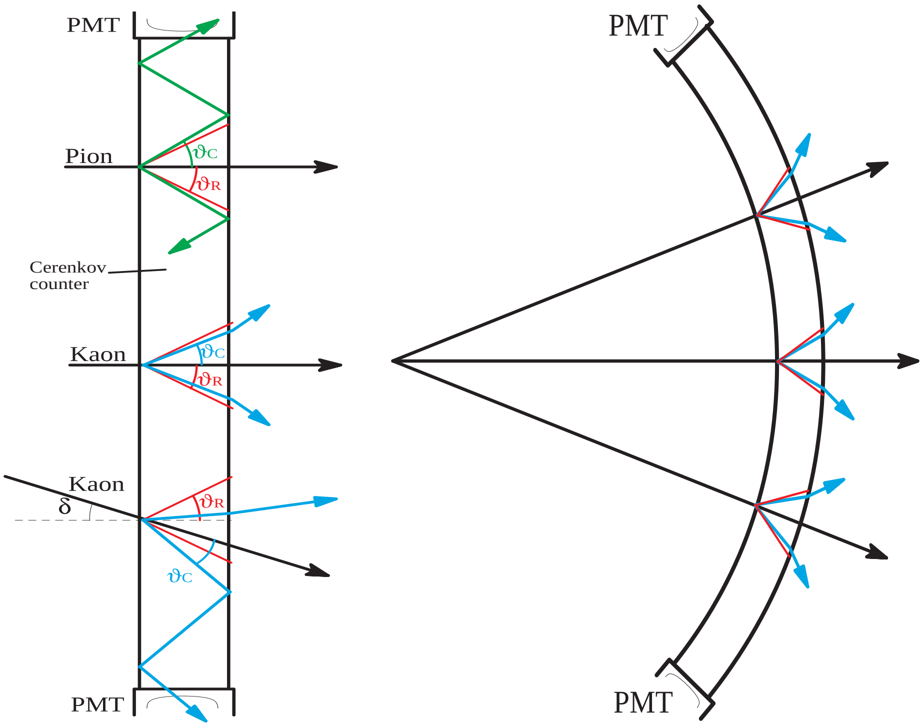

Figure 5: For Cherenkov light created by pions the Cherenkov angle ϑ_C is larger than ϑ_R, the angle of total reflection. The light is reflected back into the detector, travel up to the PMT and creates a signal. For kaons, ϑ_C is smaller than , therefore the Cherenkov light is not reflected, leaves the detector and creates no signal at the PMT. If a kaon hits the detector with an inclination $\delta > \vartheta_R$-ϑ_C, a part of the created Cherenkov light will be reflected and can reach the PMT, which has to be avoided. With a curved Cherenkov detector, perpendicular incidence for all particles at the given ANKE geometry can be achieved [31].

To provide additional separation of kaons and pions, one can use the time-of-flight between the target and the "stop"-scintillators instead of using the TOF between "start"- and "stop"-scintillators. The distance between the "start"- and "stop"-scinillators is 238 cm for a momentum of 1000 MeV/c, while the distance from the target to the same "stop"-counter is 397 cm. The difference in TOF of kaons and pions then increases from 0.84 ns to 1.40 ns allowing a clear separation of those particles only by means of TOF.

In practice, the TOF between target and “stop”-counters can be substituted by the measurement of the time difference of correlated K^+ and K^- detected in the positive and negative “stop”-counters, respectively. At this point one uses the fact, that “stop”-counters on the positive side are located in the focal surface of the spectrometer magnet, and, thus, particles passing certain “start-stop”-combination of the positive detection system have a well defined β.

3 Simulations

The ϕ-meson from $pp \rightarrow pp\phi$ reaction can be measured by reconstruction of the K^+K^- invariant mass. Obviously the non-resonant $pp \rightarrow ppK^+K^-$ reaction is the dominant background at these energies. In order to estimate the detection rates and optimize the detector setup both the $pp \rightarrow pp\phi$ and $pp \rightarrow ppK^+K^-$ reactions were simulated by Pluto [32] and ROOT [33] . The simulation results were normalized to the $pp \rightarrow pp\phi$ and $pp \rightarrow ppK^+K^-$ production cross sections.

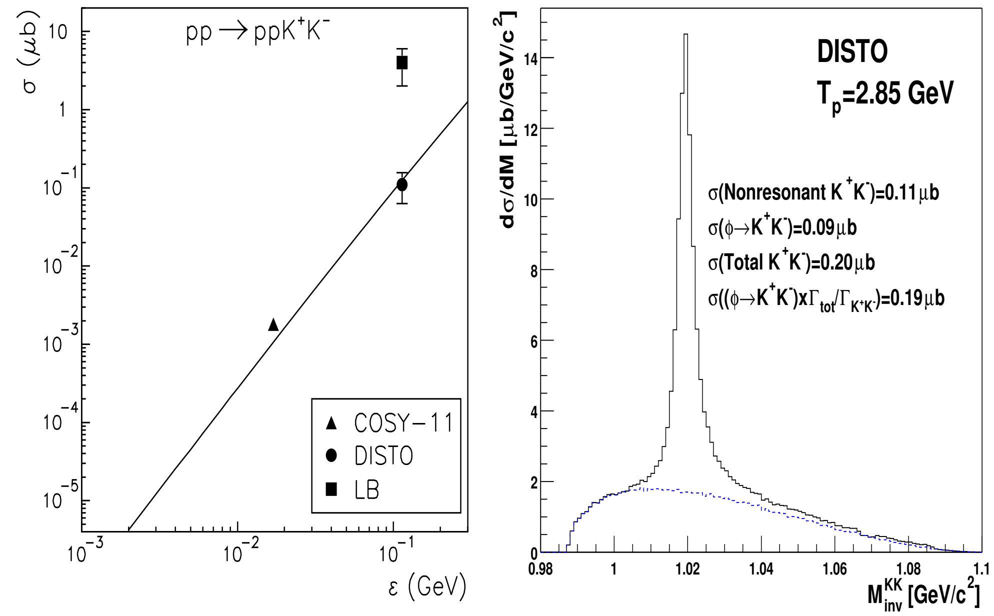

Figure 6: Left: The $pp \rightarrow ppK^+K^-$ cross section as a function of excess energy above the K^+K^- production threshold. The solid line shows the calculation from [26], data are from reference [16,25]. Right: Spectrum of invariant K^+K^- mass simulated for DISTO experimental conditions [25].

The $pp \rightarrow pp\phi$ cross section was taken from Fig.3a). The results are shown in Fig.7 for the simulation without pp FSI and with maximal enhancement due to FSI, which is shown in Fig.3a) by the solid line. Therefore the simulation results takes into account of our estimations due to the unknown $pp \rightarrow pp\phi$ cross section near the reaction threshold.

Furthermore, the $pp \to ppK^+K^-$ cross section was estimated by recent experimental data from DISTO [23] and COSY-11 [25], as well as by theoretical calculations [26], shown in the left part of Fig.6 by the solid line.

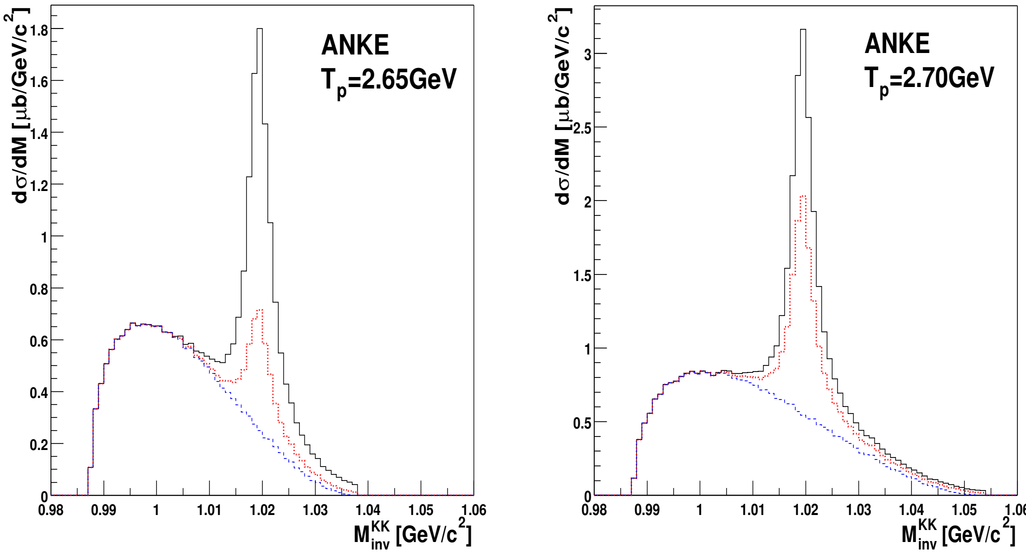

Figure 7: The expected spectra of invariant K^+K^- mass for proton beam energies $T_p = 2.65\ GeV$ and $T_p = 2.70\ GeV$. A clearly separated ϕ-signal – with and without FSI, is observed on a broad non-resonant K^+K^- distribution.

In Fig.7 the expected distributions of invariant K^+K^- mass for the two beam energies 2.65 GeV and 2.70 GeV are finally shown. Fig.8 shows tracks from kaons and protons from the following reactions: $pp \to ppK^+K^-$ and $pp \to pp\phi \to ppK^+K^-$. If one considers the particles in the middle plane only, then K^- mesons fit very well to the acceptance of the negative detector. K^+ mesons and the protons are detected in roughly 50% of cases by the range telescopes and forward detector respectively. Fig.9 shows the invariant mass of the K^+K^--system with acceptances of K^+ and K^- taken into account (left figure). On the right figure the momentum resolution of 2.5% FWHM for the K^+ and K^- is included in addition. The ϕ-meson can be clearly identified from the non-resonant K^+K^- distribution.

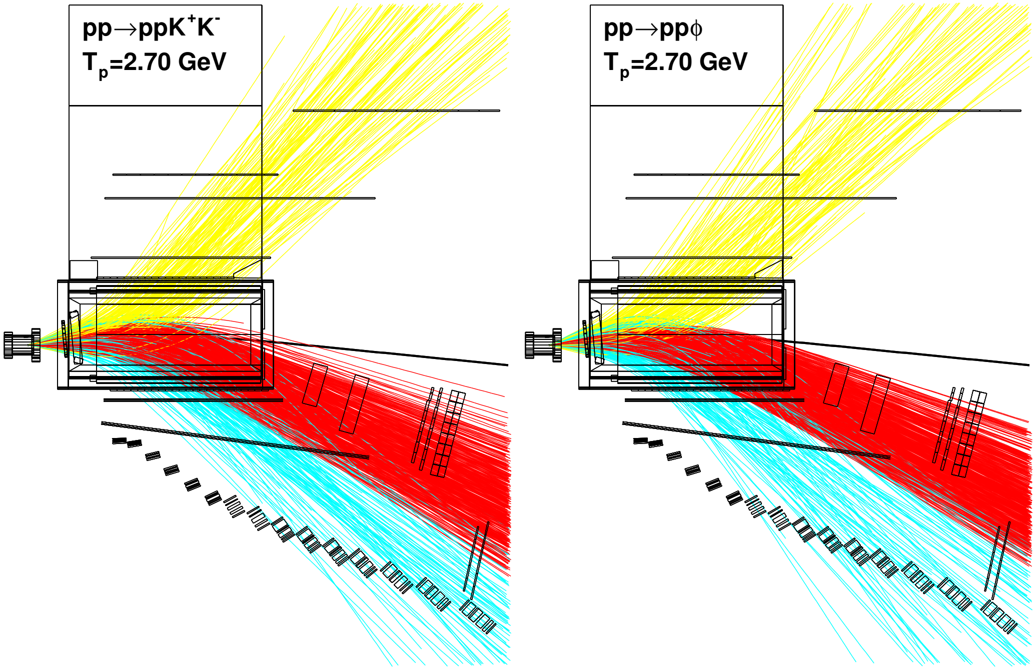

Figure 8: Kaons and protons trajectories inside the ANKE acceptance.

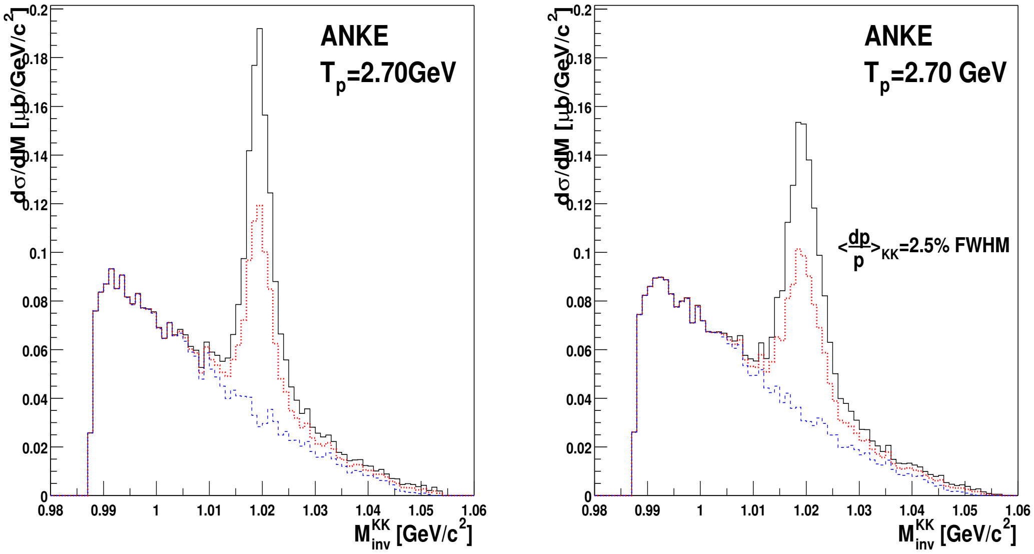

Figure 9: Spectra of invariant K^+K^- mass taking into account the K^+ and K^- detector acceptance, in addition momentum resolution is included in the right spectrum. Here, the kaon decays were not considered.

Assuming a luminosity of $L = 0.5 \cdot 10^{31}$ cm^{-2}s^{-1} – during the last ANKE beam times values larger than $1 \cdot 10^{31}$ cm^{-2}s^{-1} have been achieved – we expect for the total single rate in the positive start counters about 300000 s^{-1}. For the same rate in the negative start counters, a random coincidence rate of the two start counters of 15000 s^{-1} is expected, if the width of the coincidence window is 80 ns. If on the positive side the stop counters are included into the fast TOF on-line trigger, this rate is reduced by a factor 10. Further reduction of the count rate by a factor $\sim$ 2 is achieved by including the negative stop counters into the trigger system in addition, thus yielding a count rate of $\sim$ 750 s^{-1}. The count rates can be decreased even further by a factor of $\sim 5 - 10$ by using a triple coincidence with the forward detectors. The fast ANKE DAQ can write more than 3000 events per second to tape, thus dead time effects can be neglected.

		K^+K^--trigger	K^+K^-p-trigger
reaction *beam energy*	σ $[10^{-5}\,mb]$	*events* *in 10 days*	*events* *in 10 days*
$pp \rightarrow ppK^+K^-$			
T_p=2.65 GeV	1.8	1100	380
T_p=2.70 GeV	3.0	1800	650
$pp \rightarrow pp\phi \rightarrow ppK^+K^-$			
T_p=2.65 GeV	0.3	130	40
+ FSI	1.0	450	130
T_p=2.70 GeV	1.0	450	130
+ FSI	1.8	790	240

Table 3: Expected Number of detected events at ANKE – taking into account all efficiencies – within 10 days of data taking.

Table 3 shows the expected number of detected events for two different trigger conditions in case of non-resonant K^+K^- pairs and of ϕ-meson production for 10 days of data taking. These estimations are based on the cross sections given in Sect. 1 as well as on the previous pages (12, 13) and shown in the second column of Table 3.

For the calculation of the count rates from Table 3 all acceptances and detection efficiencies have been taken into account. The K^--detection efficiency is assumed to be 100%, whereas the efficiencies for K^+ and protons are 50% and 95%, respectively [34]. The numbers from the table show that even with the triple-coincidence as on-line trigger, sufficient statistics can be collected in order to distinguish between non-resonant K^+K^-- and ϕ-meson production. Based on the experience from previous beam times, it can be expected that background from misidentified K^+-mesons or K^+K^- can be neglected, see e.g. Appendix A of the beam request #55.2 submitted to this session of the PAC.

The protons from elastic pp-scattering in the forward detector will be used for the continuous measurement of luminosity. Technically it will be realized with a separate prescaled trigger from the forward detection system.

4 Beam time request

In total we request four weeks of beam time to measure the ϕ-meson production in pp collisions at beam energies 2.65 GeV and 2.70 GeV, by detecting the K^+K^- decay mode. These energies correspond to excess energies of 18.5 MeV and 34.6 MeV above the ϕ production threshold.

The first two weeks are requested for spring 2002 for a beam energy of 2.70 GeV. These two weeks include the time needed for calibration of the negative particle detectors at ANKE, which, for the first time, will be used for a measurement. It would be helpful to schedule this after the beam time on a_0^+-meson production (see beam-time request for proposal #55.1 submitted to this session of the PAC). During the latter, final installation and commissioning of the K^- counters is foreseen.

During the first two weeks we expect to collect about 500 K^+K^- pairs from ϕ-meson decay.

The second two weeks for the measurements at T=2.65 GeV will be requested after analyzing the data on the $pp \rightarrow pp\phi$ reaction at 2.70 GeV.

References

[1] S. Okubo, Phys. Lett. **5**, 165 (1963).

[2] G. Zweig, CERN report TH-401 (1964).

[3] J. Iizuka, Prog. Theor Phys. Suppl. **38**, 21 (1966).

[4] Particle Data Group, Eur. Phys. J. C **3**, 1 (1998).

[5] H.J. Lipkin, Phys. Lett. B **60**, 371 (1976).

[6] J. Ellis et al., Phys. Lett. B **353**, 319 (1995).

[7] A. Sibirtsev, Nucl. Phys. A **604**, 455 (1996).

[8] K. Nakayama, A. Szczurek, C. Hanhart, J. Haidenbauer and J. Speth, Phys. Rev. C **57**, 1580 (1998).

[9] K. Nakayama, J.W. Durso, J. Haidenbauer, C. Hanhart and J. Speth, Phys. Rev. C **60**, 055209 (1999).

[10] Landolt-Börnstein, *New Series* **I/12** (Springer, 1998).

[11] A. Sibirtsev and W. Cassing, Eur. Phys. J. A **7**, 403 (2000).

[12] R. Machleid, K. Holinde and Ch. Elster, Phys. Rep. **149**, 1 (1987).

[13] G. Jannseen, K. Holinde and J. Speth, Phys. Rev. C **54**, 2218 (1995).

[14] F. Hibou et al., Phys. Rev. Lett. **83**, 492 (1999).

[15] F. Balestra et al, Phys. Rev. Lett. **81**, 4572 (1998)

[16] F. Balestra et al, Phys. Rev. C **63**, 024004 (2001)

[17] S. Abd El-Samad et al, preliminary data, sub. to Nucl. Phys.

[18] V. Baru, A.M. Gasparian, J. Haidenbauer, A.E. Kudryavtsev and J. Speth, Phys. Atom. Nucl. **64**, 579 (2001).

[19] F. Hibou et al., Phys. Lett. B **438**, 41 (1998).

[20] P. Moskal et al., Phys. Rev. Lett. B **80**, 3202 (1998).

[21] P. Moskal et al., Phys. Lett. B **482**, 356 (2000).

[22] P. Moskal et al., Phys. Lett. B **474**, 416 (2000).

[23] F. Balestra et al, Phys. Lett. B **491**, 29 (2000)

[24] K. Nakayama, J. Haidenbauer and J. Speth, Phys. Rev. C **63**, 015201 (2001).

[25] C. Quentmeier et al.,Phys. Lett. B **515**, 276 (2001).

[26] A. Sibirtsev, W. Cassing and C.M. Ko, Z. Phys. A **358**, 101 (1997).

[27] V. Koptev et al., Phys. Rev. Let. volume **87**, number **2** (2001).

[28] M. Barsov et al., NIM A **462**, 364 (2001).

[29] Proposal for COSY experiment #21: "Study of subthreshold K^- production".

[30] H.R. Koch, annual report FZ-Jülich (1999) p. 28.

[31] M. Hennebach: Untersuchungen zum Einsatz von Cherenkovzählern mit Totalreflektion für die Teilchenidentifikation an ANKE, Diploma Thesis, Köln (2000); available via www.fz-juelich.de/ikp/anke.

[32] GSI, see: http://www-hades.gsi.de/computing/pluto/html/pluto.html

[33] CERN, see: http://root.cern.ch/

[34] M. Büscher et al., NIM A, in print; available via www.fz-juelich.de/ikp/anke.